

# Fractional corner charges in threefold-symmetric two-dimensional materials with fragile topology

Olga Arroyo-Gascón,<sup>1</sup> Sergio Bravo,<sup>2</sup> Leonor Chico,<sup>3</sup> and Mónica Pacheco<sup>2</sup>

<sup>1</sup>*Nanotechnology Group, USAL-Nanolab, University of Salamanca, E-37008 Salamanca, Spain*

<sup>2</sup>*Departamento de Física, Universidad Técnica Federico Santa María, Casilla 110-V, Valparaíso, Chile*

<sup>3</sup>*GISC, Departamento de Física de Materiales, Facultad de Ciencias Físicas, Universidad Complutense de Madrid, E-28040 Madrid, Spain*

(Dated: July 8, 2025)

We perform a systematic study of the signatures of fragile topology in over 50 nonmagnetic two-dimensional materials with formula  $AB_2$ , belonging to space group  $P\bar{3}m1$ . Using group theory analysis in the framework of topological quantum chemistry, we find fragile bands near the Fermi level for all the materials studied. Since stable topological bands are also present in these systems, the interplay of both phases is discussed, showing that corner charges appear in over 80% of the materials and are linked to fragile topology. Using first-principles calculations, we predict fractionally-charged corner charges protected by  $C_3$  symmetry. Our work aims to broaden the scope of materials with experimentally accessible fragile bands.

## I. INTRODUCTION

Since the proposal and subsequent discovery of the first topological insulators [1, 2], topology has enriched the electronic properties of a great number of materials. Different types of Dirac and Weyl fermions have been discovered in analogy to high-energy physics [3–5]. The development of symmetry indicators and topological quantum chemistry (TQC) [6–13] has further extended and standardized the variety of topological phases of matter. Higher-order topological insulators (HOTIs) and fragile topology are the latest additions; the former was first established in topological insulators characterized with a mirror Chern number [14, 15], while the latter has been theoretically proposed in twisted bilayer graphene [16–20]. Both phases share the absence of topological gapless modes on their surfaces or edges, in contrast to standard topological insulators. Whereas  $d$ -dimensional  $n^{\text{th}}$ -order topological insulators are known to host topological states in  $d - n$  dimensions, the same does not always apply to fragile topology. Interestingly, while nearly 90% of all classified bulk materials have at least one topological band [13, 21], only about 8% show fragile states. Thus, the search for new materials that could provide more information on signals of fragile topology is highly desirable.

Fragile topology is based on the fact that a set of fragile bands can be trivialized by adding a suitable set of trivial bands [16, 17]. The starting point for every analysis of symmetry-indicated topology is to characterize the form in which the electronic bands transform at high symmetry points in reciprocal space, under the action of the space group of the system. This allows to classify each band using the eigenvalues of the symmetry operations of the material, which corresponds to the characters (traces) of the irreducible representations (irreps). Due to real space periodicity, a set of orbitals located at specific Wyckoff positions (WP) will induce a well-defined set of irreps in the momentum space description of the

bands. The key point is that in the atomic limit, that is, no interaction among the orbitals is considered, the orbitals will induce what is called an elementary band representation (EBR). These EBRs are the building blocks that allow discriminating the type of band topology in a material [9, 10, 12]. Thus, a band is said to be topologically trivial if it can be expressed as a linear combination of EBRs where all coefficients are positive integers [10, 12]. Unlike trivial bands, fragile bands can be expressed as a combination of EBRs with integer coefficients, but at least one of them must be negative [10]. This way, when more bands are added to a fragile one, the negative EBRs can cancel out, giving rise to an all-positive linear combination of EBRs and thus trivializing the band set [8, 9, 12, 13, 16, 18, 21]. Hence, even if the fragile state is near the Fermi energy, the lower energy bands can trivialize it. This trivialization can explain the scarcity of topological materials with fragile topology features. For its part, a band has stable topology (stable upon band addition) if it can be written in terms of EBRs and at least one coefficient is fractional [8–10, 12, 13, 21].

From the above discussion, fragile topology cannot be captured by stable topological invariants such as the  $\mathbb{Z}_2$  index used in spin Hall systems. Thereby, TQC stands as one of the most useful tools to diagnose this kind of topology, together with the most general study of the evolution of Wannier charge centers along appropriate directions in reciprocal space [18, 22–27]. Beyond TQC, stable topological phases were already established in relation to the tenfold classification of systems attending to their (non-crystalline) symmetries [28] and within K-theory [29]. Note that, in a similar way, fragile phases can also arise without crystalline protection and even beyond symmetry indicators [27], as is also the case for other recently-discovered topological phases [30]. However, crystalline symmetries will play an important role in this work. In addition, although a bulk-boundary correspondence can be established for fragility using twisted boundary con-

ditions [26], this is difficult to implement in electronic systems so that a case-by-case analysis is still justified. In order to have a complete picture of fragile topological materials, a study of fragile bands for all space groups in bulk materials within the framework of TQC has been performed in Ref. [31], and high-throughput calculations have very recently classified two-dimensional materials attending to TQC and including fragile topology [32].

Fragile topology has also been theoretically reported in photonic crystals and phonon spectra [33–36]. One of its potential signatures is the presence of zero-dimensional corner states with corner charges, theoretically predicted in Refs. [20, 37, 38]. These corner charges have been theoretically reported in recent works studying different mono- and few-layered materials with diverse rotational symmetries [30, 39–49]. Moreover, higher-order Fermi arcs have also been linked to fragile and higher-order topology [50]. From an experimental point of view, fragile topology has been described in metamaterials [51–55] and quantum simulators [56], and Fermi arcs have been reported in some transition-metal dichalcogenides [57–59]. Because corner charges are a shared feature between fragile and higher-order topology, corner state measurements in real materials are often linked to the latter [60]. The potential applications of corner states as quantum dots have also been very recently highlighted, coining the concept of cornertronics [61].

It is therefore interesting to study the relation between higher-order and fragile topology. In this direction, we construct a list of two-dimensional monolayers described by space group (SG)  $P\bar{3}m1$  (164). Since transition-metal dichalcogenides (TMDs) have received a great deal of attention as candidates for layered materials with higher order [30, 41, 45, 47, 48, 62] and fragile topology [30, 50], we have focused on various TMDs, as well as on a number of non-TMDs with the same space group. We explore a total of 52 materials belonging to this SG, to find a set of experimentally suitable candidates. We demonstrate that fragile topological bands are present in all 52 materials in the region of energies near the Fermi level, and that these bands are related to the non-zero corner charges present in most of the materials and in  $C_3$ -symmetric flakes.

This article is organized as follows: in Section II, the general properties of SG 164 and the materials therein are discussed. In Section III, we compute a set of topological invariants based on the symmetry eigenvalues of the system, particularized to the TMD case studies  $ZrSe_2$ ,  $ZrS_2$  and  $SnS_2$ . In Section IV, we theoretically predict the corner charges linked to these materials and present the concept of partial corner charge. Our results are consistent with first-principles corner states calculations for triangular and hexagonal flakes in Section V.

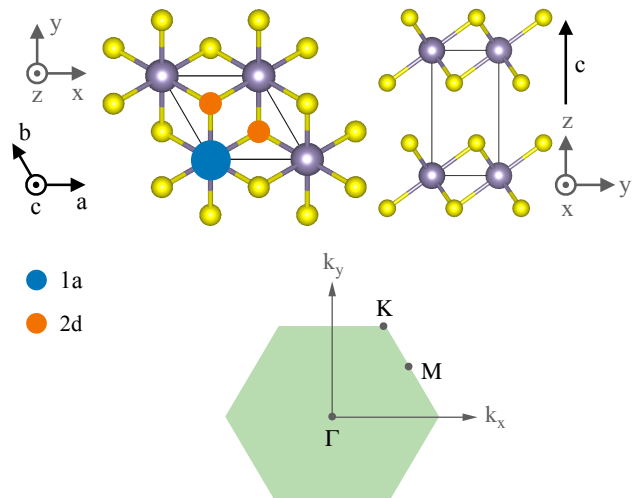


FIG. 1. Crystal structure of a unit cell belonging to SG 164: top view (upper left panel), and side view (upper right panel) displaying two layers. The structure lattice vectors, as well as the Cartesian axes, are indicated in black and gray, respectively. Blue and orange highlighted atoms indicate the 1a and 2d WPs, respectively. Bottom panel: Brillouin zone of the monolayer.

## II. COMPUTATIONAL METHODS AND GENERAL BACKGROUND OF SPACE GROUP 164 MATERIALS

Electronic structure calculations for all materials were performed using the Quantum ESPRESSO first-principles code [63, 64] employing the generalized gradient approximation (GGA) and Perdew–Burke–Ernzerhof (PBE) exchange-correlation functional. Spin-orbit coupling was considered throughout the self-consistent calculations in all cases. A kinetic energy wavefunction cutoff of 100 Ry and a  $8 \times 8 \times 1$  Monkhorst-Pack reciprocal space grid were used. All structures were relaxed until the forces were less than 0.001 eV/Å. The initial crystal structures were obtained from the Computational 2D Materials Database (C2DB) [65, 66] and checked against the Topological Materials Database [9, 13, 67] for further relaxation. Subsequently, a group theory analysis was performed using the IrRep code [68]. For the flake calculations, the SIESTA code [69, 70] was used, including spin-orbit coupling and considering the same GGA-PBE approximation.

SG 164 has inversion symmetry and includes rotational symmetries  $C_{3z}$  and  $C_{2x}$ , with a total of 12 symmetry operations. As shown in Fig. 1, we focus on  $AB_2$  compounds that display a layered structure. The A atom, which is usually (but not necessarily) a transition metal, belongs to the high-symmetry real space WP 1a, whereas the B atom is described by the 2d WP. The spatial location of these positions within the unit cell is highlighted in blue and orange, respectively, in Fig. 1. For the WPs, as well as for the symmetry operations and the SG, we

follow the notation of the Bilbao Crystallographic Server [71–73].

We screen the C2DB by restricting the search to dynamically stable monolayers with SG 164 and  $AB_2$  formula that possess a PBE band gap greater than 0.1 eV and a nonmagnetic ground state. Additionally, we also mention examples of semimetallic systems that allow for a formal definition of a set of valence bands separated from the upper conduction bands by a non-absolute gap. A complete list of materials identified in this work is presented in Table III.

In the following sections we will focus on three illustrative materials of this collection that have already been synthesized in monolayer form [74–76], namely, semiconductors  $ZrSe_2$ ,  $ZrS_2$ , and  $SnS_2$ . The semimetals  $ZrTe_2$  and  $NiTe_2$  are also briefly commented. In addition to the aforementioned compounds, other materials encompassed in this work such as  $PtSe_2$ ,  $SnI_2$ ,  $PbI_2$ ,  $PdS_2$ ,  $PtS_2$  and  $PtTe_2$  are also experimentally available as monolayers [77–81]. Note that the fragile topology database described in Ref. [31] may not apply here, since for monolayers the combination of EBRs is now restricted to the two-dimensional high-symmetry points of the Brillouin zone (BZ).

### III. BAND TOPOLOGY OF $P\bar{3}m1$ MONOLAYERS

#### A. Topological quantum chemistry analysis

We perform a TQC analysis of all individual valence bands, as well as of the full valence band manifold. The basic ingredient to start the topological description is to consider that time-reversal symmetry and spatial inversion are both preserved for all cases. This immediately implies that all bands will be twofold degenerate along the entire BZ. In addition, since spin-orbit is not negligible, double-space group irreducible representations should be employed to characterize the bands at high symmetry points. In double SG 164, the highest degeneracy that a set of bands can have is two [82], so all doubly degenerate bands will always be isolated from each other. This allows for the topological classification not only of the valence band manifold as a whole, but also for the characterization of each twofold set of bands. This basic set of bands is described by the labels of the irreps at high symmetry points  $\Gamma$ ,  $M$  and  $K$ , which comprises what is known as a band representation [9].

Following the notation in the Bilbao Crystallographic Server, we list in Table I all possible sixteen band representations that are allowed by the compatibility relations of the group. These sixteen band representations are classified as fragile, stable topological with  $\mathbb{Z}_2 = 1$ , and trivial. If a set of bands corresponds to a combination of EBRs with integer coefficients and at least one of them is negative, the set is fragile [10]; if at least one is fractional, the set has stable topology. Otherwise, if

	$\Gamma$	$M$	$K$	$Q_{c,no\ inv}$	$Q_{c,inv}$
EBR	$\bar{\Gamma}_4\bar{\Gamma}_5$	$\bar{M}_3\bar{M}_4$	$\bar{K}_4\bar{K}_5$	0	0
<b>F1</b>	$\bar{\Gamma}_4\bar{\Gamma}_5$	$\bar{M}_3\bar{M}_4$	$\bar{K}_6$	4/3	2/3
<b>S</b>	$\bar{\Gamma}_4\bar{\Gamma}_5$	$\bar{M}_5\bar{M}_6$	$\bar{K}_4\bar{K}_5$	0	3/2
<b>S</b>	$\bar{\Gamma}_4\bar{\Gamma}_5$	$\bar{M}_5\bar{M}_6$	$\bar{K}_6$	4/3	1/6
<b>S</b>	$\bar{\Gamma}_6\bar{\Gamma}_7$	$\bar{M}_3\bar{M}_4$	$\bar{K}_4\bar{K}_5$	0	1/2
<b>S</b>	$\bar{\Gamma}_6\bar{\Gamma}_7$	$\bar{M}_3\bar{M}_4$	$\bar{K}_6$	4/3	7/6
EBR	$\bar{\Gamma}_6\bar{\Gamma}_7$	$\bar{M}_5\bar{M}_6$	$\bar{K}_4\bar{K}_5$	0	0
<b>F2</b>	$\bar{\Gamma}_6\bar{\Gamma}_7$	$\bar{M}_5\bar{M}_6$	$\bar{K}_6$	4/3	2/3
<b>F3</b>	$\bar{\Gamma}_8$	$\bar{M}_3\bar{M}_4$	$\bar{K}_4\bar{K}_5$	2/3	4/3
EBR	$\bar{\Gamma}_8$	$\bar{M}_3\bar{M}_4$	$\bar{K}_6$	0	0
<b>S</b>	$\bar{\Gamma}_8$	$\bar{M}_5\bar{M}_6$	$\bar{K}_4\bar{K}_5$	2/3	5/6
<b>S</b>	$\bar{\Gamma}_8$	$\bar{M}_5\bar{M}_6$	$\bar{K}_6$	0	3/2
<b>S</b>	$\bar{\Gamma}_9$	$\bar{M}_3\bar{M}_4$	$\bar{K}_4\bar{K}_5$	2/3	11/6
<b>S</b>	$\bar{\Gamma}_9$	$\bar{M}_3\bar{M}_4$	$\bar{K}_6$	0	1/2
<b>F4</b>	$\bar{\Gamma}_9$	$\bar{M}_5\bar{M}_6$	$\bar{K}_4\bar{K}_5$	2/3	4/3
EBR	$\bar{\Gamma}_9$	$\bar{M}_5\bar{M}_6$	$\bar{K}_6$	0	0

TABLE I. Basic band representations in SG 164 monolayer, including trivial (labeled EBR), stable topological with  $\mathbb{Z}_2 = 1$  (labeled S), and fragile (labeled F and numbered). Corner charges with and without inversion symmetry are gathered in the last two columns and described in Section IV.

all coefficients are positive integers, the set is generally said to be in an atomic limit and trivial [12]. To identify these phases, we follow the Smith decomposition procedure [10] as detailed in the Supporting Information (SI) [83], and define a strong topological invariant indicated by symmetry eigenvalues  $\mathbb{Z}_2$  as

$$\mathbb{Z}_2 = c_6 \bmod 2, \quad (1)$$

where  $c_6$  is the 6-th element of the  $c$ -vector, obtained from the multiplicities of the irreps of each band set and whose computation is detailed in the SI.

We have checked that fragile and  $\mathbb{Z}_2 = 1$  bands are present near the Fermi level in all reported materials. For instance, fragile band F4 can be decomposed into EBRs as shown in Eq. 2 below:

$$F4 = -\bar{E}_{1g} @ 1a + \bar{E}_1 @ 2d. \quad (2)$$

The negative coefficients confirm the fragile nature of the band, and are also present in the rest of fragile bands in Table I. In all cases, fragile bands are described in terms of EBRs coming from WPs 1a and 2d, which are the occupied sites in the unit cell. The EBR decomposition of all fragile bands F1 - F4, as well as of an exemplary strong topological band with  $\mathbb{Z}_2 = 1$ , are explicitly stated in the SI. Note that these representations are not unique as the general formulation for the symmetry data vector has several free parameters. These parameters are usually set to zero [10]; however, we have checked that other parameter choices do not change the resulting topological nature of each symmetry data vector. A potential interplay between strong,  $\mathbb{Z}_2 = 1$ -indicated topological

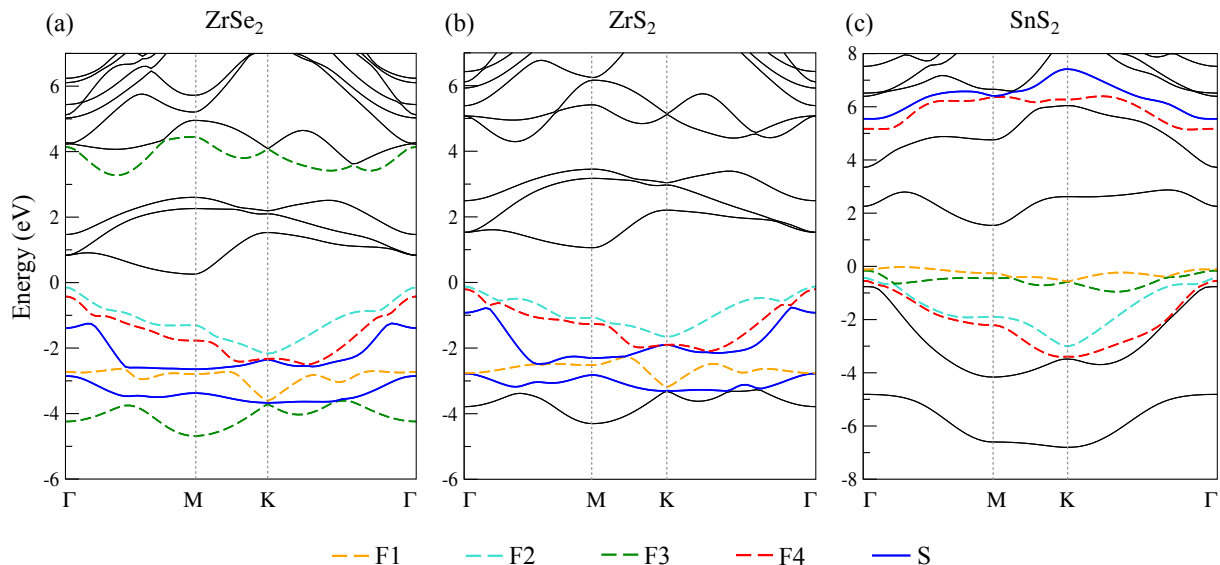


FIG. 2. Band structure of monolayer (a)  $\text{ZrSe}_2$ , (b)  $\text{ZrS}_2$  and (c)  $\text{SnS}_2$ . Fragile bands are represented in colored dashed lines, and  $\mathbb{Z}_2 = 1$  bands are highlighted in dark blue.

phases and fragile phases and its effect on corner states would be of great interest.

#### *Application to case studies*

In light of our preceding general results, we now classify the electronic bands in the representative case studies  $\text{ZrSe}_2$ ,  $\text{ZrS}_2$  and  $\text{SnS}_2$ . Fig. 2 (a) shows the band structure of monolayer  $\text{ZrSe}_2$  near the Fermi level, where a variety of topological bands, both stable and fragile, appear. All types of identified fragile bands F1, F2, F3, and F4, shown in dashed lines and different colors, are present in the valence set near the neutrality point. Stable  $\mathbb{Z}_2 = 1$  bands, highlighted in dark blue, also appear in the valence region and have been broadly labeled S for simplicity. If we extend the TQC analysis to the entire valence band set, we find that  $\text{ZrSe}_2$  is topologically trivial, as the total set of irreps is expressed as a sum of different EBRs; the EBR decomposition of the full valence set is detailed in the SI. This is consistent with the intuitive notion of fragile bands: they are trivialized when combined with others. However, the  $\mathbb{Z}_2 = 1$  bands remain topological upon addition; the only exception is the addition of an even number of  $\mathbb{Z}_2 = 1$  bands, since the  $\mathbb{Z}_2$  index is defined modulo 2. We emphasize that there are more topologically stable and fragile bands at lower energies, which we do not show in the figure, but have been taken into consideration in order to compute the topological properties of the valence band set.

$\text{ZrSe}_2$  and  $\text{ZrS}_2$  are semiconductors and share almost the same topological band distribution for the uppermost valence bands, as seen in Fig. 2 (a) and (b). In both cases, the first, second, and fourth valence bands are fragile, and the third and fifth valence bands are sta-

ble topological with  $\mathbb{Z}_2 = 1$ . In fact, the band structure has an overall similar appearance for both materials, as expected since they belong to a similar chemical environment. However, in  $\text{ZrS}_2$  there are no topological bands in the conduction set near the Fermi level. As in  $\text{ZrSe}_2$ , all valence bands add up to a trivial topological invariant.

Figure 2 (c) displays an analogous band structure for the semiconductor  $\text{SnS}_2$ . As in  $\text{ZrSe}_2$ , all fragile bands F1, F2, F3, and F4 found in Table I are present in the figure. Interestingly, this Fig. does not include any  $\mathbb{Z}_2 = 1$  bands; however, we have found such bands at lower energies. As in the previous cases, the whole valence manifold is topologically trivial, as explicitly detailed in the SI.

For the rest of the monolayers studied, the results are similar. Additional figures highlighting fragile and stable bands for  $\text{ZrTe}_2$  and  $\text{NiTe}_2$  are found in the SI. They both have a higher density of stable bands but show fragile states near the Fermi level. Since  $\text{ZrTe}_2$  and  $\text{NiTe}_2$  are semimetals, we have set the uppermost valence band to match previous works [9, 13, 67].  $\text{ZrTe}_2$  is the only material studied with a topologically nontrivial valence band set, with  $\mathbb{Z}_2 = 1$ , in agreement with experimental reports of Dirac-like edge states [84]. In fact, all the materials mentioned above ( $\text{ZrSe}_2$ ,  $\text{ZrS}_2$ ,  $\text{SnS}_2$ ,  $\text{ZrTe}_2$  and  $\text{NiTe}_2$ ) are experimentally feasible in monolayer form.

### **B. Symmetry-indicator invariants beyond topological quantum chemistry**

The former TQC analysis yields a broad range of materials with fragile and stable topological bands; however, we find that fragile bands become trivialized at the Fermi level. Moreover, even though a  $\mathbb{Z}_2$  invariant is computed

for stable topological bands, an invariant for fragile bands would also be useful to fully characterize the topological features of our system. A set of symmetry-indicator topological invariants, applicable to systems protected by crystalline (mainly rotational) symmetries, has been introduced in Refs. [38, 39]. These invariants are computed in terms of certain symmetry eigenvalues of the system at selected high-symmetry points, and therefore characterize diverse topological phases, such as second-order HOTIs, fragile topology, or obstructed atomic limits [39].

In order to compute the corresponding symmetry-indicator invariants for our materials, we notice that all the studied monolayers belong to layer group  $p\bar{3}m1$ . Following Ref. [39], we focus on  $C_3$  and inversion symmetries, present in layer group  $p\bar{3}m1$ , in order to define a topological invariant for such a system in the presence of spin-orbit coupling:

$$\nu_{inv} = (M_{-1}^I, K_{-1}^3), \quad (3)$$

where  $M_{-1}^I$  is the difference between the number of states at  $M$  and  $\Gamma$  points with inversion eigenvalue  $-1$ . Analogously,  $K_{-1}^3$  is the difference between the number of states at  $K$  and  $\Gamma$  points with  $C_3$  eigenvalue  $-1$ . We will use  $\nu_{inv}$  to characterize finite geometries that retain the monolayer point group ( $\bar{3}m$ ), and also explore the case of a system in which inversion symmetry is absent, leaving  $3m$  as the point group of the structure. For this configuration,  $\nu_{no\ inv}$  is the appropriate invariant to describe the topological properties:

$$\nu_{no\ inv} = (K_{e^{i\pi/3}}^3, K_{-1}^3), \quad (4)$$

where  $K_{e^{i\pi/3}}^3$  is the difference of number of states at  $K$  and  $\Gamma$  with  $C_3$  eigenvalue  $e^{i\pi/3}$ .

The inversion-breaking scenario requires further elaboration because we are reducing the number of crystalline symmetries. To relate the topological classification developed for SG 164 to this reduced case, we must study how the irreps of this SG map to the SG without inversion, which is SG 156 ( $P\bar{3}m1$ ). As this is a subgroup of index 2 of SG 164, we can employ the subduction procedure, as explained in Ref. [10]. The result of this map can be extracted from the Bilbao Crystallographic Server, and for completeness, it is also presented in the SI. Most importantly, this map preserves the fragility of the SG 164 bands. Moreover, bands with stable topology in SG 164 are mapped to either EBRs (if the  $K_{-1}^3$  invariant is zero) or fragile bands (if the  $K_{-1}^3$  invariant is nonzero) in SG 156. The prevalence of fragility in SG 156 is also confirmed by the Smith decomposition procedure for this group, as it does not host stable  $\mathbb{Z}_2$  phases that can be diagnosed by symmetry indicators alone (there can, however, exist other stable topological phases, as the system belongs to the class AII of the Altland–Zirnbauer classification [28]).

AB <sub>2</sub>	#M <sub>-1</sub> <sup>I</sup>	#Γ <sub>-1</sub> <sup>I</sup>	#K <sub>-1</sub> <sup>3</sup>	#Γ <sub>-1</sub> <sup>3</sup>	ν <sub>inv</sub>
ZrSe <sub>2</sub>	24	24	14	14	(0, 0)
ZrS <sub>2</sub>	14	14	8	6	(0, 2)
SnS <sub>2</sub>	8	8	10	8	(0, 2)

AB <sub>2</sub>	#K <sub>e<sup>iπ/3</sup></sub> <sup>3</sup>	#Γ <sub>e<sup>iπ/3</sup></sub> <sup>3</sup>	#K <sub>-1</sub> <sup>3</sup>	#Γ <sub>-1</sub> <sup>3</sup>	ν <sub>no inv</sub>
ZrSe <sub>2</sub>	15	15	14	14	(0, 0)
ZrS <sub>2</sub>	8	9	8	6	(-1, 2)
SnS <sub>2</sub>	8	9	10	8	(-1, 2)

TABLE II. Symmetry indicator invariants related to fractional corner charges in SG 164 monolayer unit cell with (top part) and without (bottom part) inversion symmetry.

#### Application to case studies

Table II collects both symmetry indicators  $\nu_{inv}$  and  $\nu_{no\ inv}$  for the valence band set of the selected compounds ZrSe<sub>2</sub>, ZrS<sub>2</sub>, and SnS<sub>2</sub>. Although the TQC analysis presented in the previous section yielded a trivial valence band set for all three compounds, nontrivial symmetry-indicator invariants are obtained for all cases except ZrSe<sub>2</sub>. This is expected, since symmetry-indicator invariants successfully characterize topological phases whose bands at the Fermi level are an apparently trivial sum of EBRs, such as fragile topology and obstructed atomic limits. It follows that symmetry indicators are especially useful in our systems. Crucially, a nonzero  $\nu_{inv}$  anticipates the presence of fractional corner charges in  $C_3 + I$ -symmetric materials under open boundary conditions, whereas a nonzero  $\nu_{no, inv}$  indicates a similar behavior for  $C_3$ -symmetric systems [38, 39].

On a different note, symmetry-indicator invariants are also related to the Wilson loop spectra of the bands [39], which, due to the presence of crystalline symmetries, can be computed using the corresponding eigenvalues. As a general result for all the structures studied, we find that all fragile bands present a zero  $M_{-1}^I$  invariant, which indicates a nonwinding Wilson loop along the  $\Gamma - M$  direction. This is the usual path for the characterization of the  $\mathbb{Z}_2$  topology and indicates that fragile bands will show a trivial character along that direction even when their WL spectra are calculated in isolation from other bands. Nevertheless, as has been made patent in previous works [24, 25, 40, 44, 85], fragility can be captured by other different paths, a fact that the nonzero values of  $K_{e^{i\pi/3}}^3$  and  $K_{-1}^3$  corroborate. These invariants are related to the  $\Gamma - K$  path, which implies that fragile bands have nontrivial features that will show in responses related to these indicators.

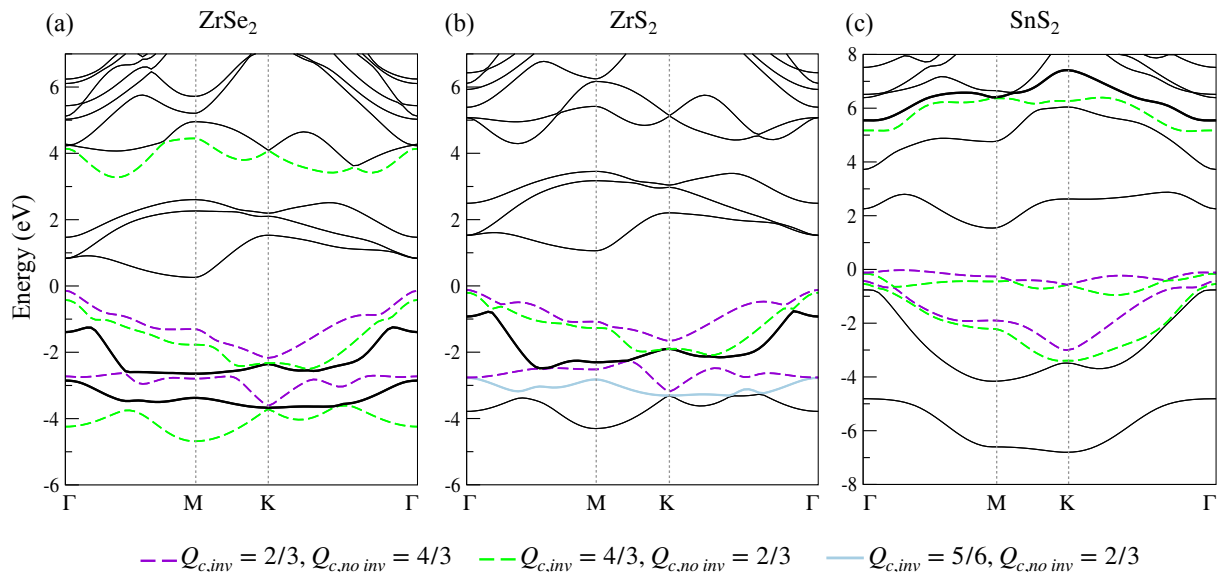


FIG. 3. Band structure of monolayer (a) ZrSe<sub>2</sub>, (b) ZrS<sub>2</sub> and (c) SnS<sub>2</sub> with bands with nonzero partial corner charges colored in green and purple, respectively. Bands with ill-defined corner charges are colored gray. Fragile bands are represented with dashed lines, and stable topological bands are highlighted with thick lines.

#### IV. CORNER CHARGE ANALYSIS

In an open system, fractional corner charges are a signature of topology stemming from a filling anomaly, which arises at charge neutrality when enforcing certain crystalline symmetries in topological systems [38, 39, 86–88]. These systems can be trivial under periodic boundary conditions, but not under open conditions, where robust, fractionally-filled corner states appear [39, 50]. In particular, in the presence of  $C_3$  and inversion symmetry, the corner charge  $Q_{c,inv}$  hosted at each  $C_3$ -symmetric sector of a flake is defined in terms of the symmetry-indicator invariants defined in Section III as [39]

$$Q_{c,inv} = -\frac{1}{4}M_{-1}^I - \frac{1}{3}K_{-1}^3 \text{ mod } 2. \quad (5)$$

The allowed charge values for the three equal threefold symmetric corners, besides zero, are  $1/3$ ,  $2/3$ ,  $1$ ,  $4/3$ , or  $5/3$ . In the absence of inversion, the corner charge  $Q_{c,no inv}$  reads

$$Q_{c,no inv} = \frac{2}{3}K_{e^{i\pi/3}}^3 + \frac{2}{3}K_{-1}^3 \text{ mod } 2. \quad (6)$$

This implies three equal corner charges with values  $2/3$  or  $4/3$ . These formulas hold in the presence of spin-orbit coupling. For both the inversion-preserving and the inversion-breaking cases, the presence of spin-orbit coupling and time-reversal symmetry ensures that all states are at least twofold degenerate due to the Kramers' theorem, which leads to the aforementioned allowed values for  $Q_{c,inv}$  and  $Q_{c,no inv}$  [38, 39].

It is worthwhile to emphasize the non-uniqueness of the corner charge value [38], since the filling anomaly at

the neutrality point can be overcome by either filling or depleting the Fermi level. In the following, we will work in units of the fundamental charge of the electron, and therefore assume that a corner charge of  $n/N$  indicates that each  $N$ -symmetric sector of the system would need  $n$  additional electrons for the states at the neutrality point to be completely filled. This convention has also been explicitly followed in previous works [89].

In this way, it is straightforward to predict the presence of corner charges  $Q_{c,inv}$  and  $Q_{c,no inv}$  in candidate materials from standard first-principles calculations. The existence of corner charges, that could be observed via STM measurements, is key for the experimental identification of novel types of topology such as HOTIs and fragile systems. The relevance of corner charges is further highlighted since, as discussed in the Introduction, realizations of fragile topology are elusive, but nonzero  $Q_{c,inv}$  or  $Q_{c,no inv}$  would confirm that the fragility of these systems could be overcome in an open boundary setting.

However, as already commented in Refs. [38, 39], symmetry-indicator invariants and corner charges are a shared property between second-order HOTIs, fragile systems, and obstructed atomic limits. In fact, besides stable and fragile bands, some SG 164 monolayers also show obstructed atomic insulator behavior [90, 91]. Symmetry-indicator invariants  $\nu_{c,inv}$  and  $\nu_{c,no inv}$  do not distinguish between the aforementioned topological phases, since they are the same for all of them. Nevertheless, the presence of corner charges is mostly linked to HOTIs in the literature. Therefore, we aim to know whether the potential (well-defined) corner states are exclusively related to fragile topology in SG 164 monolay-

ers or not. To this end, we follow two equivalent approaches. First, we compute a partial corner charge, which is the application of the above equations for  $Q_{c,inv}$  and  $Q_{c,no\,inv}$  to each set of doubly degenerate bands. Thus, we can identify which bands contribute to the total corner charge, and from the TQC analysis of Section III A, the type of topology they host. Second, we obtain the total value of the corner charges for the complete valence band set, which results from the addition (modulo 2) of the partial corner charges.

*Application to case studies*

We first present the result of the partial corner charge approach in panels (a), (b), and (c) of Figure 3 for  $ZrSe_2$ ,  $ZrS_2$  and  $SnS_2$ , respectively. All three materials present fragile bands with well-defined nonzero corner charges  $Q_{c,inv}$  and  $Q_{c,no\,inv}$  near the Fermi level, which could be accessed individually in principle by doping processes. Analogous Figs. for semimetals  $ZrTe_2$  and  $NiTe_2$  can be found in the SI.

In Table I we present a summary of the computed partial corner charges for the sixteen types of basic band representations. It is readily observed that EBRs do not carry any partial corner charges, and that all the nonzero values stem from fragile and topologically stable bands. In particular, in the case with no inversion, as from Section III B only fragile bands are present in SG 156, a nonzero total corner charge is exclusively associated with the presence of uncompensated (fragile) partial corner charges.

On the other hand, when inversion is present, fragile bands individually have a well-defined fractional corner charge according to the definition [38, 39], whereas stable bands present corner charges that are not among the allowed values of Eq. 5 and thus could not give rise to the corresponding filling anomaly. This is the case, for example, of the fifth valence band of  $ZrS_2$  in Figure 3 (b). However, the sum of an even number of stable topological bands (which will trivialize the  $\mathbb{Z}_2$  invariant) results in a direct sum of EBRs and fragile bands, with a well-defined joint partial corner charge. For instance, the sum of the fifth and eighth stable bands in Table I, both present in  $ZrS_2$ , is

$$\begin{aligned} S5 + S8 &= (\bar{\Gamma}_9 \oplus \bar{M}_3\bar{M}_4 \oplus \bar{K}_6) \oplus (\bar{\Gamma}_8 \oplus \bar{M}_5\bar{M}_6 \oplus \bar{K}_4\bar{K}_5) \\ &= (\bar{\Gamma}_9 \oplus \bar{M}_5\bar{M}_6 \oplus \bar{K}_6) \oplus (\bar{\Gamma}_8 \oplus \bar{M}_3\bar{M}_4 \oplus \bar{K}_4\bar{K}_5) \\ &= \text{EBR} + \text{F3}. \end{aligned} \tag{7}$$

This set has a corner charge  $Q_{c,inv} = 4/3$ , which is a well-defined value and the same as that of fragile band F3. We have checked that this holds for all pairwise additions of strong bands in Table I. Moreover, even when partial corner charges stemming from fragile bands are trivialized mod 2 and the only contribution to  $Q_{c,inv}$  is that of stable bands, these stable bands always come

A	B = Chalcogen			
Zr	ZrO <sub>2</sub>	<b>ZrS<sub>2</sub></b>	<b>ZrSe<sub>2</sub></b>	ZrTe <sub>2</sub>
Sn	SnO <sub>2</sub>	<b>SnS<sub>2</sub></b>	SnSe <sub>2</sub>	
Ni	NiO <sub>2</sub>	NiS <sub>2</sub>		<b>NiTe<sub>2</sub></b>
Pt	PtO <sub>2</sub>	PtS <sub>2</sub>	PtSe <sub>2</sub>	PtTe <sub>2</sub>
Hf	HfO <sub>2</sub>	HfS <sub>2</sub>	HfSe <sub>2</sub>	
Pd	PdO <sub>2</sub>	PdS <sub>2</sub>	PdSe <sub>2</sub>	
Si			SiSe <sub>2</sub>	
Pb	PbO <sub>2</sub>	PbS <sub>2</sub>		
Ge	GeO <sub>2</sub>	GeS <sub>2</sub>		

A	B = Halogen			
Cd	CdI <sub>2</sub>	CdBr <sub>2</sub>	CdCl <sub>2</sub>	CdF <sub>2</sub>
Zn	ZnI <sub>2</sub>	ZnBr <sub>2</sub>	ZnCl <sub>2</sub>	ZnF <sub>2</sub>
Pb	PbI <sub>2</sub>	PbBr <sub>2</sub>	PbCl <sub>2</sub>	
Ru	RuI <sub>2</sub>	RuBr <sub>2</sub>	RuCl <sub>2</sub>	
Hg				HgF <sub>2</sub>
Mg	MgI <sub>2</sub>	MgBr <sub>2</sub>		
Ca	CaI <sub>2</sub>	CaBr <sub>2</sub>		
Sr	SrI <sub>2</sub>	SrBr <sub>2</sub>		
Ba	BaI <sub>2</sub>	BaBr <sub>2</sub>		
Os	OsI <sub>2</sub>	OsBr <sub>2</sub>		
Sn	SnI <sub>2</sub>			
Ge	GeI <sub>2</sub>			

TABLE III. List of all the materials studied in the database, sorted by the elements A and B in their formula  $AB_2$ . The exemplary materials discussed in the main text and the SI are highlighted in bold text. Compounds highlighted in green have  $Q_{c,inv} = 4/3$  and  $Q_{c,no\,inv} = 2/3$ , in gray  $Q_{c,inv}$  is not well defined, and the rest have no corner charges.

in pairs so that their joint contribution equals a sum of EBRs and fragile bands. Detailed calculations that support this statement can be found in the SI for several materials.

It follows that the origin of the corner charges in this SG is related to fragile topology, even when  $\mathbb{Z}_2 = 1$  bands are considered. Even when the whole valence band manifold is trivialized from a TQC perspective, corner states can appear.

We have verified that the sum of partial charges equals the corner charge obtained by applying Eqs. 5 and 6 for the whole set of valence bands for the five materials highlighted in this work. The results for all the valence bands for each material are gathered in Table III. For all materials in our database, well-defined corner charges  $Q_{c,inv} = 4/3$  or  $Q_{c,inv} = 0$ , and  $Q_{c,no\,inv} = 2/3$  or  $Q_{c,no\,inv} = 0$  are found, except for  $ZrTe_2$ , that has an ill-defined  $Q_{c,inv} = 5/6$ . This is consistent with the fact that  $ZrTe_2$  is stable topological with  $\mathbb{Z}_2 = 1$  and hosts Dirac cones, which hamper the presence of a filling anomaly at the neutrality point. Moreover, over 80% of the samples have non-zero corner charges.

However, we have found that all halogen-based materials show a mismatch between the computed  $Q_{c,inv} = 4/3$ ,  $Q_{c,no\,inv} = 2/3$  and the actual filling anomaly inferred from their flake eigenvalue spectra, as demonstrated in

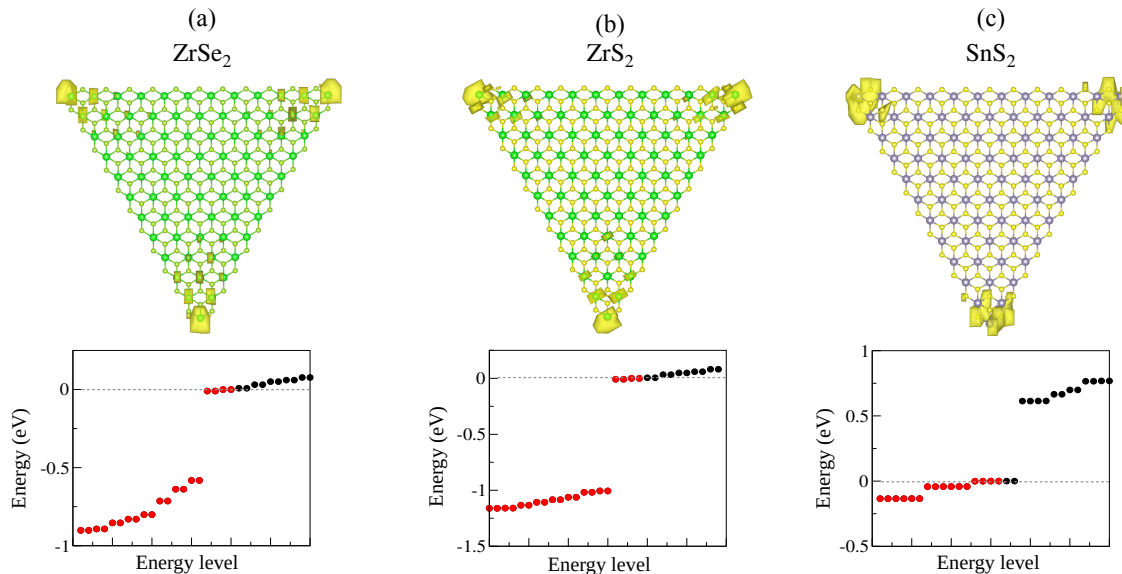


FIG. 4. LDOS (top panel) and eigenvalue spectra (bottom panel) for the (a)  $\text{ZrSe}_2$ , (b)  $\text{ZrS}_2$  and (c)  $\text{SnS}_2$  triangular flakes.

the SI for  $\text{MgBr}_2$ . Namely, by counting the number of filled states at the neutrality point, we find that flakes involving halogens should have  $Q_{c,inv} = 5/3$  and  $Q_{c,no\,inv} = 4/3$ .

Even though chalcogen- and halogen-based SG 164 monolayers have identical crystalline symmetries, they do not host the same number of filled states at the neutrality point. This difference in the filling anomaly value stems from the fact that the 2d WP in chalcogen-based materials has no atomic support in real space, whereas for halogen-based systems it has partial support [91]. In fact, the fractional corner charge of a system can be foreseen from symmetry arguments based on the real-space distribution of Wannier functions [22, 38, 39], and SG 164 monolayers also host a topological orbital-obstructed atomic insulator phase [90, 91]. It follows that, unlike stable topological bands (whose effect on corner charges could be traced back to fragile bands), orbital-obstructed topology plays a major role along with fragile topology in the emergence of corner states in SG 164 monolayers. The trivialization of the fragile bands at the Fermi level, where obstructed atomic insulators are diagnosed, impedes to study both topological phases separately. Since for chalcogen-based materials fractional corner charges can be determined solely from crystalline symmetry arguments and a more detailed study of the number and disposition of the valence electrons is needed for halogen systems, in the following we will focus on the former and leave the latter for a different study [91]. Overall, for materials with no atomic support at the 2d WP, the arguments presented in this work are valid.

Besides the three highlighted systems, other materials with nonzero fractional charges are  $\text{PdS}_2$ ,  $\text{SnS}_2$  or  $\text{PtS}_2$ , which are synthesized in monolayer form and constitute

interesting experimental candidates for STM measurements of corner charges.

## V. CORNER STATES IN FLAKES

In contrast to most materials hosting fragile topology, SG 164 does not have  $C_{2z}$  symmetry, so our fragile bands must be protected by other symmetry operations. Following our previous reasoning, we propose two flake geometries, a hexagonal one with  $C_3$  symmetry and inversion, and a triangular one with  $C_3$  but without inversion. The latter is the most simple approach since the triangular flake breaks not only the inversion but also the  $C_2$  symmetries, having point group symmetry  $3m$ . For its part, the hexagonal flake preserves all monolayer symmetries, with point group symmetry  $\bar{3}m$ .

For the triangular flake, a high electronic localization is observed via first-principles local density of states (LDOS) calculations at the three corners of Fig. 4 for the selected materials  $\text{ZrSe}_2$ ,  $\text{ZrS}_2$ , and  $\text{SnS}_2$ . Since a band gap is necessary for well-defined corner charges, semimetals  $\text{ZrTe}_2$  and  $\text{NiTe}_2$  are not considered here.

In the bottom panel of Fig. 4, the flake eigenvalues depict a sixfold degeneracy at the Fermi level. Note that the states are not exactly localized at the Fermi level due to the absence of chiral symmetry [44]. DFT simulations also take into account potential interactions between corner states [92], which contribute to the elimination of degeneracy. This size effect is reduced by increasing the flake size; in fact, the number of degenerate states at the neutrality point can change depending on the system size, although the value of filled states is left unchanged (see SI). Such degeneracy is best observed the larger the

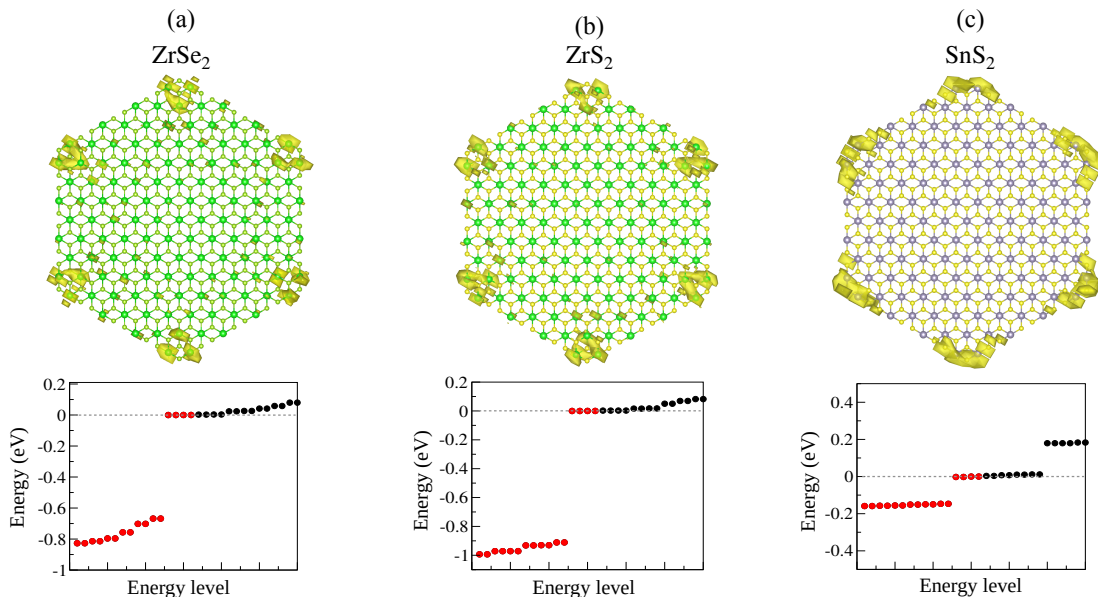


FIG. 5. LDOS (top panel) and eigenvalue spectra (bottom panel) for the (a)  $\text{ZrSe}_2$ , (b)  $\text{ZrS}_2$  and (c)  $\text{SnS}_2$  hexagonal flakes.

band gap is, as verified by considering that  $\text{SnS}_2$  has the largest gap of all three materials, and also comparing with Fig. 3 in the SI for  $\text{MgBr}_2$  (with a gap over three times larger than  $\text{SnS}_2$ ).

To fill this sixfold degeneracy, two additional electrons are needed for each material; therefore, each corner of the triangle should contribute  $2/3$  (in units of the electron charge). From Table III, both  $\text{ZrS}_2$  and  $\text{SnS}_2$  have a corner charge without inversion  $Q_{c, no\ inv} = 2/3$ , in agreement with the value obtained by inspection of the eigenvalue spectra. The only exception is  $\text{ZrSe}_2$ , whose eigenvalue spectra yields  $Q_{c, no\ inv} = 2/3$  but has a computed  $Q_{c, no\ inv} = 0$  from Table III. This is due to the trivialization of partial corner charges by the extra low-lying valence bands that are considered within our DFT framework for Se-based alloys, and that are absent in other different DFT approaches [32].

Fig. 5 shows the LDOS and energy spectra of hexagonal flakes with  $C_3 + I$  symmetry. As in Fig. 4, there are four filled states at the neutrality point; however, now degeneracies are increased due to the presence of inversion symmetry. Namely, the spectrum is 12-fold degenerate at the Fermi level; this is best seen for flakes with larger band gaps whose edge states sit higher in energy, such as  $\text{SnS}_2$  in panel (c). In fact, panels (a), (b) and (c) are ordered by increasing band gap. In order to fill the Fermi level, 8 extra electrons would be needed, yielding  $Q_{c, inv} = 4/3$  per corner of the flake. This value is in agreement with our previous calculations of the corner charge in Table III. Additional hexagonal flake figures are shown in the SI for smaller systems, emphasizing the need for sizable flakes in order to obtain robust degeneracies.

## VI. CONCLUSIONS

SG 164 monolayer systems span a great variety of structures, which motivates a thorough search for non-trivial topological properties in this family. A comprehensive selection of compounds with  $\text{AB}_2$  formula was surveyed, and the case studies  $\text{ZrSe}_2$ ,  $\text{ZrS}_2$  and  $\text{SnS}_2$  were selected for a detailed description. Our general results indicate the presence of stable ( $\mathbb{Z}_2 = 1$ ) and fragile topological bands. Thus, SG 164 is an interesting platform to study the interplay between fragile and stable topology and its experimental implications, and where other topological phases such as orbital-obstructed atomic insulator behavior have also been reported.

Using first-principles calculations, we have analyzed the symmetry eigenvalues of the topologically nontrivial bands in these materials and computed their corner charges and related invariants. We have found nonzero topological indices for more than 80% of the screened materials. A detailed analysis of partial corner charges, computed for each band, has proven fundamental in clarifying the role of stable topological and fragile bands. Whereas these fractional charges are usually related to higher-order topology, we show that, in many SG 164 monolayers, corner charges are closely related to fragile bands. Moreover, via irrep subduction to the SG 156, we demonstrate that the nontrivial character of the fragility-induced topological invariants must be preserved in configurations where inversion is explicitly broken. Halogen-based monolayers are an exception, since the predicted corner charges are not in agreement with subsequent flake calculations. For these materials, a real-space analysis following an orbital-obstructed study can correctly foresee corner charges, and fragile topology plays a secondary

role.

These findings were therefore tested mainly on non-halogen compounds, and using triangular and hexagonal geometries. For triangular flakes, a filling anomaly was identified for the three exemplary materials, resulting in a corner charge valued  $2/3$ . Regarding hexagonal structures, we find a corner charge of  $4/3$ . Both values agree with our previous analytical calculations.

It can also be noted that as the nontrivial results depend on the  $3m1$  symmetry, materials with a bulk structure described by SG 156 are likely to present the same effects. Examples of this are Janus TMDs, which are seen as an attractive platform for extending and applying the results achieved in this work. In summary, a direct link was established between  $C_3$  symmetry-protected corner charges and fragile topology in a wide set of two-dimensional materials. The universality of our findings among SG 164, and possibly other SGs sharing the relevant threefold symmetry, encourages the experimental realization of responses bound to fragile topology in real materials.

#### ACKNOWLEDGEMENTS

The authors thank J. D. Correa for helpful discussions. We acknowledge the financial support of the Agencia Estatal de Investigación of Spain under grant PID2022-136285NB-C31 and from the Comunidad de Madrid through the (MAD2D-CM)-UCM5 project, funded by the Recovery, Transformation and Resilience Plan, and

by NextGenerationEU from the European Union. O.A.G acknowledges the support of grant PRE2019-088874 funded by MCIN/AEI/10.13039/501100011033 and by “ESF Investing in your future”, and of European Union NextGenerationEU/PRTR project Consolidación Investigadora CNS2022-136025, as well as Instituto de Ciencia de Materiales de Madrid (ICMM-CSIC) and Universidad Complutense de Madrid, where this project was initiated. S.B. acknowledges the support of the Postdoctoral Grant from the Universidad Técnica Federico Santa María. M. P. acknowledges the financial support of Chilean FONDECYT by grant 1211913. Finally, we thank the Centro de Supercomputación de Galicia, CESGA, ([www.cesga.es](http://www.cesga.es), Santiago de Compostela, Spain) and Supercomputación Castilla y León (SCAYLE) for providing access to their supercomputing facilities.

#### SUPPORTING INFORMATION

The Supporting Information is available at <http://link.aps.org/supplemental/10.1103/qcr8-jxvn>.

It includes topological quantum chemistry analysis of SG 164 monolayers, as well as additional figures for topological semimetals  $ZrTe_2$  and  $NiTe_2$  and other flake figures. The irreducible representations and symmetry operations at high symmetry points of all the valence bands of the 52 materials studied using Quantum ESPRESSO and the IrRep code are available and can be downloaded as a zip file.

- 
- [1] M. Z. Hasan and C. L. Kane, Colloquium: Topological insulators, *Reviews of Modern Physics* **82**, 3045–3067 (2010).
- [2] X.-L. Qi and S.-C. Zhang, Topological insulators and superconductors, *Reviews of Modern Physics* **83**, 1057–1110 (2011).
- [3] T. Wehling, A. Black-Schaffer, and A. Balatsky, Dirac materials, *Advances in Physics* **63**, 1–76 (2014).
- [4] S.-Y. Xu, I. Belopolski, N. Alidoust, M. Neupane, G. Bian, C. Zhang, R. Sankar, G. Chang, Z. Yuan, C.-C. Lee, S.-M. Huang, H. Zheng, J. Ma, D. S. Sanchez, B. Wang, A. Bansil, F. Chou, P. P. Shibayev, H. Lin, S. Jia, and M. Z. Hasan, Discovery of a weyl fermion semimetal and topological fermi arcs, *Science* **349**, 613–617 (2015).
- [5] N. Armitage, E. Mele, and A. Vishwanath, Weyl and dirac semimetals in three-dimensional solids, *Reviews of Modern Physics* **90**, 015001 (2018).
- [6] L. Fu and C. L. Kane, Topological insulators with inversion symmetry, *Physical Review B* **76**, 045302 (2007).
- [7] H. C. Po, A. Vishwanath, and H. Watanabe, Symmetry-based indicators of band topology in the 230 space groups, *Nature Communications* **8**, 50 (2017).
- [8] J. Kruthoff, J. de Boer, J. van Wezel, C. L. Kane, and R.-J. Slager, Topological classification of crystalline insulators through band structure combinatorics, *Phys. Rev. X* **7**, 041069 (2017).
- [9] B. Bradlyn, L. Elcoro, J. Cano, M. G. Vergniory, Z. Wang, C. Felser, M. I. Aroyo, and B. A. Bernevig, Topological quantum chemistry, *Nature* **547**, 298 (2017).
- [10] L. Elcoro, Z. Song, and B. A. Bernevig, Application of induction procedure and Smith decomposition in calculation and topological classification of electronic band structures in the 230 space groups, *Physical Review B* **102**, 035110 (2020).
- [11] H. C. Po, Symmetry indicators of band topology, *Journal of Physics: Condensed Matter* **32**, 263001 (2020).
- [12] J. Cano and B. Bradlyn, Band representations and Topological Quantum Chemistry, *Annual Review of Condensed Matter Physics* **12**, 225 (2021).
- [13] M. G. Vergniory, B. J. Wieder, L. Elcoro, S. S. P. Parkin, C. Felser, B. A. Bernevig, and N. Regnault, All topological bands of all nonmagnetic stoichiometric materials, *Science* **376**, eabg9094 (2022).
- [14] J. C. Y. Teo, L. Fu, and C. L. Kane, Surface states and topological invariants in three-dimensional topological insulators: Application to  $Bi_{1-x}Sb_x$ , *Physical Review B* **78**, 045426 (2008).
- [15] F. Schindler, A. M. Cook, M. G. Vergniory, Z. Wang, S. S. P. Parkin, B. A. Bernevig, and T. Neupert,

- Higher-order topological insulators, *Science Advances* **4**, eaat0346 (2018).
- [16] H. C. Po, H. Watanabe, and A. Vishwanath, Fragile topology and Wannier obstructions, *Phys. Rev. Lett.* **121**, 126402 (2018).
- [17] L. Zou, H. C. Po, A. Vishwanath, and T. Senthil, Band structure of twisted bilayer graphene: Emergent symmetries, commensurate approximants, and Wannier obstructions, *Phys. Rev. B* **98**, 085435 (2018).
- [18] Z. Song, Z. Wang, W. Shi, G. Li, C. Fang, and B. A. Bernevig, All Magic Angles in Twisted Bilayer Graphene are Topological, *Physical Review Letters* **123**, 036401 (2019).
- [19] H. C. Po, L. Zou, T. Senthil, and A. Vishwanath, Faithful tight-binding models and fragile topology of magic-angle bilayer graphene, *Physical Review B* **99**, 195455 (2019).
- [20] J. Ahn, S. Park, and B.-J. Yang, Failure of Nielsen-Ninomiya theorem and fragile topology in two-dimensional systems with space-time inversion symmetry: Application to twisted bilayer graphene at magic angle, *Phys. Rev. X* **9**, 021013 (2019).
- [21] B. J. Wieder, B. Bradlyn, J. Cano, Z. Wang, M. G. Vergniory, L. Elcoro, A. A. Soluyanov, C. Felser, T. Neupert, N. Regnault, and B. A. Bernevig, Topological materials discovery from crystal symmetry, *Nature Reviews Materials* **7**, 196 (2022).
- [22] W. A. Benalcazar, B. A. Bernevig, and T. L. Hughes, Electric multipole moments, topological multipole moment pumping, and chiral hinge states in crystalline insulators, *Phys. Rev. B* **96**, 245115 (2017).
- [23] J. Cano, B. Bradlyn, Z. Wang, L. Elcoro, M. G. Vergniory, C. Felser, M. I. Aroyo, and B. A. Bernevig, Topology of disconnected elementary band representations, *Physical Review Letters* **120**, 266401 (2018).
- [24] B. Bradlyn, Z. Wang, J. Cano, and B. A. Bernevig, Disconnected elementary band representations, fragile topology, and Wilson loops as topological indices: An example on the triangular lattice, *Physical Review B* **99**, 045140 (2019).
- [25] A. Bouhon, A. M. Black-Schaffer, and R.-J. Slager, Wilson loop approach to fragile topology of split elementary band representations and topological crystalline insulators with time-reversal symmetry, *Phys. Rev. B* **100**, 195135 (2019).
- [26] Z.-D. Song, L. Elcoro, and B. A. Bernevig, Twisted bulk-boundary correspondence of fragile topology, *Science* **367**, 794 (2020).
- [27] A. Bouhon, T. Bzdušek, and R.-J. Slager, Geometric approach to fragile topology beyond symmetry indicators, *Phys. Rev. B* **102**, 115135 (2020).
- [28] A. Altland and M. R. Zirnbauer, Nonstandard symmetry classes in mesoscopic normal-superconducting hybrid structures, *Physical Review B* **55**, 1142 (1997).
- [29] A. Kitaev, V. Lebedev, and M. Feigel'man, Periodic table for topological insulators and superconductors, *AIP Conference Proceedings* **1134**, 22 (2009).
- [30] Z. Wang, B. J. Wieder, J. Li, B. Yan, and B. A. Bernevig, Higher-order topology, monopole nodal lines, and the origin of large Fermi arcs in transition metal dichalcogenides  $XTe_2$  ( $X = Mo, W$ ), *Physical Review Letters* **123**, 186401 (2019).
- [31] Z.-D. Song, L. Elcoro, Y.-F. Xu, N. Regnault, and B. A. Bernevig, Fragile Phases as Affine Monoids: Classification and Material Examples, *Physical Review X* **10**, 031001 (2020).
- [32] U. Petralanda, Y. Jiang, B. A. Bernevig, N. Regnault, and L. Elcoro, Two-dimensional topological quantum chemistry and catalog of topological materials (2024), arXiv:cond-mat/2411.08950v1.
- [33] M. B. de Paz, M. G. Vergniory, D. Bercioux, A. García-Etxarri, and B. Bradlyn, Engineering fragile topology in photonic crystals: Topological quantum chemistry of light, *Physical Review Research* **1**, 032005 (2019).
- [34] J. L. Mañes, Fragile phonon topology on the honeycomb lattice with time-reversal symmetry, *Physical Review B* **102**, 024307 (2020).
- [35] Y. Wei, B. Yan, Y. Peng, A. Shi, D. Zhao, R. Peng, Y. Xiang, and J. Liu, Fragile topology in double-site honeycomb lattice photonic crystal, *Optics Letters* **46**, 3941 (2021).
- [36] Y. Wang, S. Xu, L. Feng, and R. Agarwal, Design of fragile topological flat bands in an optical microcavity array, *Phys. Rev. B* **110**, 045401 (2024).
- [37] B. J. Wieder and B. A. Bernevig, The Axion Insulator as a Pump of Fragile Topology arXiv.1810.02373 (2018).
- [38] W. A. Benalcazar, T. Li, and T. L. Hughes, Quantization of fractional corner charge in  $C_n$ -symmetric higher-order topological crystalline insulators, *Physical Review B* **99**, 245151 (2019).
- [39] F. Schindler, M. Brzezińska, W. A. Benalcazar, M. Iraola, A. Bouhon, S. S. Tsirkin, M. G. Vergniory, and T. Neupert, Fractional corner charges in spin-orbit coupled crystals, *Physical Review Research* **1**, 033074 (2019).
- [40] S. Kobayashi and A. Furusaki, Fragile topological insulators protected by rotation symmetry without spin-orbit coupling, *Physical Review B* **104**, 195114 (2021).
- [41] J. Zeng, H. Liu, H. Jiang, Q.-F. Sun, and X. C. Xie, Multiorbital model reveals a second-order topological insulator in 1 H transition metal dichalcogenides, *Physical Review B* **104**, L161108 (2021).
- [42] S. Kooi, G. Van Miert, and C. Ortix, The bulk-corner correspondence of time-reversal symmetric insulators, *npj Quantum Materials* **6**, 1 (2021).
- [43] A. Skurativska, S. S. Tsirkin, F. D. Natterer, T. Neupert, and M. H. Fischer, Flat bands with fragile topology through superlattice engineering on single-layer graphene, *Phys. Rev. Res.* **3**, L032003 (2021).
- [44] A. Luo, Z. Song, and G. Xu, Fragile topological band in the checkerboard antiferromagnetic monolayer FeSe, *npj Computational Materials* **8**, 26 (2022).
- [45] S. Qian, G.-B. Liu, C.-C. Liu, and Y. Yao,  $C_n$ -symmetric higher-order topological crystalline insulators in atomically thin transition metal dichalcogenides, *Physical Review B* **105**, 045417 (2022).
- [46] Y.-F. Chen and D.-X. Yao, Fragile topological phase on the triangular kagome lattice and its bulk-boundary correspondence, *Physical Review B* **107**, 155129 (2023).
- [47] M. Costa, B. Focassio, L. M. Canonico, T. P. Cysne, G. R. Schleder, R. B. Muniz, A. Fazzio, and T. G. Rappoport, Connecting Higher-Order Topology with the Orbital Hall Effect in Monolayers of Transition Metal Dichalcogenides, *Physical Review Letters* **130**, 116204 (2023).
- [48] G. Liu, H. Jiang, Z. Guo, X. Zhang, L. Jin, C. Liu, and Y. Liu, Magnetic Second-Order Topological Insulators in 2H-Transition Metal Dichalcogenides, *Advanced Science* **10**, 2301952 (2023).
- [49] V. Nuñez, S. Bravo, J. D. Correa, L. Chico, and

- M. Pacheco, Higher-order obstructed atomic insulator phase in pentagonal monolayer PdSe<sub>2</sub>, *2D Materials* **11**, 015015 (2023).
- [50] B. J. Wieder, Z. Wang, J. Cano, X. Dai, L. M. Schoop, B. Bradlyn, and B. A. Bernevig, Strong and fragile topological Dirac semimetals with higher-order Fermi arcs, *Nature Communications* **11**, 627 (2020).
- [51] V. Peri, Z.-D. Song, M. Serra-Garcia, P. Engeler, R. Queiroz, X. Huang, W. Deng, Z. Liu, B. A. Bernevig, and S. D. Huber, Experimental characterization of fragile topology in an acoustic metamaterial, *Science* **367**, 797 (2020).
- [52] F. N. Ünal, A. Bouhon, and R.-J. Slager, Topological Euler class as a dynamical observable in optical lattices, *Phys. Rev. Lett.* **125**, 053601 (2020).
- [53] B. Jiang, A. Bouhon, Z.-K. Lin, X. Zhou, B. Hou, F. Li, R.-J. Slager, and J.-H. Jiang, Experimental observation of non-abelian topological acoustic semimetals and their phase transitions, *Nature Physics* **17**, 1239–1246 (2021).
- [54] Y. Wu, Z.-K. Lin, Y. Yang, Z. Song, F. Li, and J.-H. Jiang, Probing fragile topology with dislocations, *Science Bulletin* **69**, 3657–3660 (2024).
- [55] B. Jiang, A. Bouhon, S.-Q. Wu, Z.-L. Kong, Z.-K. Lin, R.-J. Slager, and J.-H. Jiang, Observation of an acoustic topological euler insulator with meronic waves, *Science Bulletin* **69**, 1653–1659 (2024).
- [56] W. Zhao, Y.-B. Yang, Y. Jiang, Z. Mao, W. Guo, L. Qiu, G. Wang, L. Yao, L. He, Z. Zhou, Y. Xu, and L. Duan, Quantum simulation for topological Euler insulators, *Communications Physics* **5**, 223 (2022).
- [57] D. Rhodes, R. Schönemann, N. Aryal, Q. Zhou, Q. R. Zhang, E. Kampert, Y.-C. Chiu, Y. Lai, Y. Shimura, G. T. McCandless, J. Y. Chan, D. W. Paley, J. Lee, A. D. Finke, J. P. C. Ruff, S. Das, E. Manousakis, and L. Balicas, Bulk Fermi surface of the Weyl type-II semimetallic candidate  $\gamma$ -MoTe<sub>2</sub>, *Physical Review B* **96**, 165134 (2017).
- [58] D. Di Sante, P. K. Das, C. Bigi, Z. Ergönenc, N. Gürtler, J. A. Krieger, T. Schmitt, M. N. Ali, G. Rossi, R. Thomale, C. Franchini, S. Picozzi, J. Fujii, V. N. Strocov, G. Sangiovanni, I. Vobornik, R. J. Cava, and G. Panaccione, Three-Dimensional Electronic Structure of the Type-II Weyl Semimetal WTe<sub>2</sub>, *Physical Review Letters* **119**, 026403 (2017).
- [59] Y. Wu, N. H. Jo, D. Mou, L. Huang, S. L. Bud'ko, P. C. Canfield, and A. Kaminski, Three-dimensionality of the bulk electronic structure in WTe<sub>2</sub>, *Physical Review B* **95**, 195138 (2017).
- [60] F. Schindler, Z. Wang, M. G. Vergniory, A. M. Cook, A. Murani, S. Sengupta, A. Y. Kasumov, R. Deblock, S. Jeon, I. Drozdov, H. Bouchiat, S. Guéron, A. Yazdani, B. A. Bernevig, and T. Neupert, Higher-order topology in bismuth, *Nature Physics* **14**, 918 (2018).
- [61] Y. Han, C. Cui, X.-P. Li, T.-T. Zhang, Z. Zhang, Z.-M. Yu, and Y. Yao, Cornertronics in two-dimensional second-order topological insulators, *Physical Review Letters* **133**, 176602 (2024).
- [62] G. Long, M. Pan, H. Zeng, and H. Huang, Second-order topological insulators in two-dimensional monolayers of the 1T-phase PtSe<sub>2</sub> material class, *Phys. Rev. Mater.* **8**, 044203 (2024).
- [63] P. Giannozzi, S. Baroni, N. Bonini, M. Calandra, R. Car, C. Cavazzoni, D. Ceresoli, G. L. Chiarotti, M. Cococcioni, I. Dabo, A. D. Corso, S. de Gironcoli, S. Fabris, G. Fratesi, R. Gebauer, U. Gerstmann, C. Gougoussis, A. Kokalj, M. Lazzeri, L. Martin-Samos, N. Marzari, F. Mauri, R. Mazzarello, S. Paolini, A. Pasquarello, L. Paulatto, C. Sbraccia, S. Scandolo, G. Sclauzero, A. P. Seitsonen, A. Smogunov, P. Umari, and R. M. Wentzcovitch, QUANTUM ESPRESSO: A modular and open-source software project for quantum simulations of materials, *Journal of Physics: Condensed Matter* **21**, 395502 (2009).
- [64] P. Giannozzi, O. Andreussi, T. Brumme, O. Bunau, M. B. Nardelli, M. Calandra, R. Car, C. Cavazzoni, D. Ceresoli, M. Cococcioni, N. Colonna, I. Carnimeo, A. D. Corso, S. de Gironcoli, P. Delugas, R. A. DiStasio, A. Ferretti, A. Floris, G. Fratesi, G. Fugallo, R. Gebauer, U. Gerstmann, F. Giustino, T. Gorni, J. Jia, M. Kawamura, H.-Y. Ko, A. Kokalj, E. Küçükbenli, M. Lazzeri, M. Marsili, N. Marzari, F. Mauri, N. L. Nguyen, H.-V. Nguyen, A. Otero-de-la-Roza, L. Paulatto, S. Poncé, D. Rocca, R. Sabatini, B. Santra, M. Schlipf, A. P. Seitsonen, A. Smogunov, I. Timrov, T. Thonhauser, P. Umari, N. Vast, X. Wu, and S. Baroni, Advanced capabilities for materials modelling with Quantum ESPRESSO, *Journal of Physics: Condensed Matter* **29**, 465901 (2017).
- [65] S. Haastруп, M. Strange, M. Pandey, T. Deilmann, P. S. Schmidt, N. F. Hinsche, M. N. Gjerding, D. Torelli, P. M. Larsen, A. C. Riis-Jensen, J. Gath, K. W. Jacobsen, J. J. Mortensen, T. Olsen, and K. S. Thygesen, The Computational 2D Materials Database: High-throughput modeling and discovery of atomically thin crystals, *2D Materials* **5**, 042002 (2018).
- [66] M. N. Gjerding, A. Taghizadeh, A. Rasmussen, S. Ali, F. Bertoldo, T. Deilmann, N. R. Knøsgaard, M. Kruse, A. H. Larsen, S. Manti, T. G. Pedersen, U. Petralanda, T. Skovhus, M. K. Svendsen, J. J. Mortensen, T. Olsen, and K. S. Thygesen, Recent progress of the Computational 2D Materials Database (C2DB), *2D Materials* **8**, 044002 (2021).
- [67] M. G. Vergniory, L. Elcoro, C. Felser, N. Regnault, B. A. Bernevig, and Z. Wang, A complete catalogue of high-quality topological materials, *Nature* **566**, 480 (2019).
- [68] M. Iraola, J. L. Mañes, B. Bradlyn, M. K. Horton, T. Neupert, M. G. Vergniory, and S. S. Tsirkin, IrRep: Symmetry eigenvalues and irreducible representations of ab initio band structures, *Computer Physics Communications* **272**, 108226 (2022).
- [69] J. M. Soler, E. Artacho, J. D. Gale, A. García, J. Junquera, P. Ordejón, and D. Sánchez-Portal, The SIESTA method for ab initio order-N materials simulation, *Journal of Physics: Condensed Matter* **14**, 2745 (2002).
- [70] A. García, N. Papior, A. Akhtar, E. Artacho, V. Blum, E. Bosoni, P. Brandimarte, M. Brandbyge, J. I. Cerdá, F. Corsetti, R. Cuadrado, V. Dikan, J. Ferrer, J. Gale, P. García-Fernández, V. M. García-Suárez, S. García, G. Huhs, S. Illera, R. Korytár, P. Koval, I. Lebedeva, L. Lin, P. López-Tarifa, S. G. Mayo, S. Mohr, P. Ordejón, A. Postnikov, Y. Pouillon, M. Pruneda, R. Robles, D. Sánchez-Portal, J. M. Soler, R. Ullah, V. W.-z. Yu, and J. Junquera, Siesta: Recent developments and applications, *The Journal of Chemical Physics* **152**, 204108 (2020).
- [71] M. I. Aroyo, A. Kirov, C. Capillas, J. M. Perez-Mato, and H. Wondratschek, Bilbao Crystallographic Server. II. Representations of crystallographic point groups and

- space groups, *Acta Crystallographica Section A Foundations of Crystallography* **62**, 115 (2006).
- [72] M. I. Aroyo, J. M. Perez-Mato, C. Capillas, E. Kroumova, S. Ivantchev, G. Madariaga, A. Kirov, and H. Wondratschek, Bilbao Crystallographic Server: I. Databases and crystallographic computing programs, *Zeitschrift für Kristallographie - Crystalline Materials* **221**, 15 (2006).
- [73] M. Aroyo, J. Perez-Mato, D. Orobengoa, E. Tasci, G. De La Flor, and A. Kirov, *Crystallography online: Bilbao Crystallographic Server*, *Bulgarian Chemical Communications* **43**, 183 (2011).
- [74] M. Zhang, Y. Zhu, X. Wang, Q. Feng, S. Qiao, W. Wen, Y. Chen, M. Cui, J. Zhang, C. Cai, and L. Xie, Controlled Synthesis of ZrS<sub>2</sub> Monolayer and Few Layers on Hexagonal Boron Nitride, *Journal of the American Chemical Society* **137**, 7051 (2015).
- [75] S. Mañas-Valero, V. García-López, A. Cantarero, and M. Galbiati, Raman Spectra of ZrS<sub>2</sub> and ZrSe<sub>2</sub> from Bulk to Atomically Thin Layers, *Applied Sciences* **6**, 264 (2016).
- [76] G. Ye, Y. Gong, S. Lei, Y. He, B. Li, X. Zhang, Z. Jin, L. Dong, J. Lou, R. Vajtai, W. Zhou, and P. M. Ajayan, Synthesis of large-scale atomic-layer SnS<sub>2</sub> through chemical vapor deposition, *Nano Research* **10**, 2386 (2017).
- [77] Y. Wang, L. Li, W. Yao, S. Song, J. T. Sun, J. Pan, X. Ren, C. Li, E. Okumishi, Y.-Q. Wang, E. Wang, Y. Shao, Y. Y. Zhang, H.-t. Yang, E. F. Schwier, H. Iwasawa, K. Shimada, M. Taniguchi, Z. Cheng, S. Zhou, S. Du, S. J. Pennycook, S. T. Pantelides, and H.-J. Gao, Monolayer PtSe<sub>2</sub>, a New Semiconducting Transition-Metal-Dichalcogenide, Epitaxially Grown by Direct Selenization of Pt, *Nano Letters* **15**, 4013 (2015).
- [78] S. Sinha, T. Zhu, A. France-Lanord, Y. Sheng, J. C. Grossman, K. Porfyrakis, and J. H. Warner, Atomic structure and defect dynamics of monolayer lead iodide nanodisks with epitaxial alignment on graphene, *Nature Communications* **11**, 823 (2020).
- [79] E. Chen, W. Xu, J. Chen, and J. H. Warner, 2D layered noble metal dichalcogenides (Pt, Pd, Se, S) for electronics and energy applications, *Materials Today Advances* **7**, 100076 (2020).
- [80] Q.-Q. Yuan, F. Zheng, Z.-Q. Shi, Q.-Y. Li, Y.-Y. Lv, Y. Chen, P. Zhang, and S.-C. Li, Direct Growth of van der Waals Tin Diiodide Monolayers, *Advanced Science* **8**, 2100009 (2021).
- [81] L. Liu, D. Zemlyanov, and Y. P. Chen, Epitaxial growth of monolayer PdTe<sub>2</sub> and patterned PtTe<sub>2</sub> by direct telurization of Pd and Pt surfaces, *2D Materials* **8**, 045033 (2021).
- [82] L. Elcoro, B. Bradlyn, Z. Wang, M. G. Vergniory, J. Cano, C. Felser, B. A. Bernevig, D. Orobengoa, G. de la Flor, and M. I. Aroyo, Double crystallographic groups and their representations on the bilbao crystallographic server, *Journal of Applied Crystallography* **50**, 1457–1477 (2017).
- [83] See Supplemental Material at <http://link.aps.org/supplemental/10.1103/qcr8-jxvn> for topological quantum chemistry analysis of SG 164 monolayers, as well as additional figures for topological semimetals ZrTe<sub>2</sub> and NiTe<sub>2</sub> and other flake figures. The irreducible representations and symmetry operations at high symmetry points of all the valence bands of the 52 materials studied using Quantum ESPRESSO and the IrRep code are available and can be downloaded as a zip file.
- [84] P. Tsipas, D. Tsoutsou, S. Fragkos, R. Sant, C. Alvarez, H. Okuno, G. Renaud, R. Alcotte, T. Baron, and A. Dimoulas, Massless Dirac Fermions in ZrTe<sub>2</sub> Semimetal Grown on InAs(111) by van der Waals Epitaxy, *ACS Nano* **12**, 1696 (2018).
- [85] J. Henke, M. Kurttutan, J. Kruthoff, and J. van Wezel, Topological invariants of rotationally symmetric crystals, *Phys. Rev. B* **104**, L201110 (2021).
- [86] E. Lee, R. Kim, J. Ahn, and B.-J. Yang, Two-dimensional higher-order topology in monolayer graphdiyne, *npj Quantum Materials* **5**, 1 (2020).
- [87] E. Khalaf, W. A. Benalcazar, T. L. Hughes, and R. Queiroz, Boundary-obstructed topological phases, *Physical Review Research* **3**, 013239 (2021).
- [88] M. Hitomi, T. Kawakami, and M. Koshino, Multiorbital edge and corner states in black phosphorene, *Phys. Rev. B* **104**, 125302 (2021).
- [89] J. Sodequist, U. Petralanda, and T. Olsen, Abundance of second order topology in c3 symmetric two-dimensional insulators, *2D Materials* **10**, 015009 (2022).
- [90] H. Sheng, Y. Xie, Q. Wu, H. Weng, X. Dai, B. A. Bernevig, Z. Fang, and Z. Wang, Majorana corner modes in unconventional monolayers of the 1T-PtSe<sub>2</sub> family, *Physical Review B* **110** (2024).
- [91] O. Arroyo-Gascon, S. Bravo, M. Pacheco, and L. Chico, Two-dimensional orbital-obstructed insulators with higher-order band topology (2024), arXiv:2412.09561v1.
- [92] B. Liu, G. Zhao, Z. Liu, and Z. F. Wang, Two-Dimensional Quadrupole Topological Insulator in  $\gamma$ -Graphyne, *Nano Letters* **19**, 6492 (2019).